



Geometric influence of the laser-based powder bed fusion process in Ti6AL4V and AlSi10Mg

Zhong Yang Chua^{1,2} · Seung Ki Moon² · Lishi Jiao³ · Il Hyuk Ahn⁴

Received: 1 June 2020 / Accepted: 13 April 2021 / Published online: 21 April 2021
© The Author(s), under exclusive licence to Springer-Verlag London Ltd., part of Springer Nature 2021

Abstract

Many studies have shown that the mechanical properties and geometric accuracy of additive manufacturing parts are dependent of many factors such as laser energy density, build orientation, and heat transfer histories. Amongst the factors, heat transfer histories are highly dependent on the geometry of a part, resulting in influencing the mechanical properties and microstructure evolution due to the repeated heating and cooling process. Heat transfer histories are associated with material thermal properties which include thermal conductivity, thermal diffusivity, specific heat capacity, and temperature gradient. The objective of this paper is to understand and observe the microstructure evolution process and microhardness based on variation in geometrical characteristic of the laser-based powder bed fusion (L-PBF). This paper presents the effect of the geometric factors on the mechanical properties and geometric accuracy during the L-PBF process, which benefit future process optimisation and modelling. In this study, samples with varying wall thickness are fabricated in Ti6AL4V and AlSi10Mg alloys by L-PBF. The samples are systematically evaluated by the optical microscope and the Vickers hardness tester. Microstructural characterisation of these samples is further evaluated via scanning electron microscopy. The results show that there is a significant relationship between material thermal properties, microstructure evolution, and mechanical properties with respect to the variation in wall thickness. These results can be used to understand the material thermal behaviour in lattice structures with a thin or small-sized feature and serve as a design guideline to indirectly control the microstructure of a L-PBF part.

Keywords Additive manufacturing · 3D printing · Laser-based powder bed fusion · Vickers hardness · Ti-6Al-4V · AlSi10Mg

✉ Seung Ki Moon
skmoon@ntu.edu.sg

Zhong Yang Chua
chua_zhong_yang@ite.edu.sg

Lishi Jiao
JIAO0011@e.ntu.edu.sg

Il Hyuk Ahn
ahnih@tu.ac.kr

¹ Institute of Technical Education, School of Engineering (Mechanical Engineering), ITE College East, 10 Simei Avenue, Singapore 486047, Singapore

² Singapore Centre for 3D Printing, School of Mechanical and Aerospace Engineering, Nanyang Technological University, 50 Nanyang Avenue, Singapore 639798, Singapore

³ Hebei Key Laboratory of Material Near-Net Forming Technology, School of Materials Science and Engineering, Hebei University of Science and Technology, Shijiazhuang 050018, China

⁴ Department of Mechanical Engineering, Tongmyong University, Busan 48520, South Korea

1 Introduction

Additive manufacturing (AM) has shown great potential in areas such as aerospace, biomedical and marine industries [1]. AM is a process whereby the material is added layer upon layer in order to form a 3D model, and this process is completely different from subtractive manufacturing methodologies [2]. Unlike traditional machining, AM provides numerous advantages which complex and customised parts can be produced easily, reduction in fabrication time, and flexibility to be used for repair application [3, 4]. Due to these advantages, design for additive manufacturing (DFAM) can be incorporated with various materials in traditional design for manufacturing (DFM).

One of the common metal AM processes that has been used in industrial and prototyping application is laser-based powder bed fusion (L-PBF). L-PBF is an established powder bed fusion process that utilised a high laser power to melt and fuse the powder to produce near full density 3D part. During the process, the powder is deposited by the recoating mechanism,

and once the layer has completed, the platform will be lowered down, and the powder is deposited again for the next layer. This process is repeated until the AM part is completed. The materials that are widely used for L-PBF are stainless steel, Ti6Al4V, and AlSi10Mg.

The L-PBF process involves many process factors that may affect the final quality of the fabricated parts. And extensive researches have been conducted on the L-PBF process to enhance the quality and mechanical properties of the final part through optimisation of process parameters. The quality of the L-PBF parts is closely correlated with the geometry of the melt track and is significantly dependable on four main parameters: laser power, layer thickness, scanning speed, and hatch spacing [5–14]. Ahn et al. [5] proposed an experimental approach to measure the geometry of the molten pool and investigated the correlation between the hatch spacing and the quality of the L-PBF part (geometrical accuracy and microhardness). Dadbakhsh et al. [6] identified the effect of layer thickness, scanning speed, and laser power on the microstructural evolution of L-PBF parts and showed that the optimal process parameters to achieve high quality (better microhardness property) Al matrix composites were low layer thickness, high laser power, and low scanning speed. This effect was noticed in the fabrication of Ti6Al4V L-PBF samples. Shi et al. [9] presented that an ideal molten pool geometry was achieved by low scanning speed and high laser power, and layer thickness was a key factor in deciding the degree of surface roughness. Surface finishing and densification of the L-PBF part were also dependable on scanning speed and laser power and this was investigated by Koutiri et al. [7], and the result showed that the surface roughness increased with lower scanning speed and decreased with higher laser power. Yadroitsev et al. [10] showed the correlation between the hatch spacing parameters and geometric characteristic of the melt pool. It was concluded that hatch distance would cause an effect on the geometric characteristics of melt tracks, as well as surface properties. The research was then continued to investigate and established the relationship between the L-PBF process parameters, powder metallurgy, and the geometry of single tracks via theoretical approach, Analysis of Variance (ANOVA). Ozel et al. also presented that the surface texture relationships between process parameters and resulting surface characteristics are further quantified as average track width and track-to-track overlap as related to energy density [11]. The experiment results concluded that the most influential parameter was the laser power, and to achieve better quality of the L-PBF parts, it was critical to ensure that the melted track was stable with high depth penetration [15]. The interaction of the process parameters will have a combination effect to the final property of the printed part. For the L-PBF process, the laser power density (E) can be also another main factor affecting the solidification process and is a function of the following important parameters: laser power, scanning

speed, hatch spacing and layer thickness. Some studies have proved that laser energy density is the most critical parameter in the L-PBF process as the thermal gradient and solidification of L-PBF is mainly influenced by the process parameters such as laser power and scanning speed. Li et al. [16] developed a 3-D finite element model to investigate the thermal behaviour and heat transfer during the L-PBF process based on two critical parameters: laser power and scan speed. And the simulation results were supported by experimental results. The optimal geometry of L-PBF AlSi10Mg molten pool and the best metallurgical bonding between layers were obtained at the laser power of 250W and scanning speed of 200mm/s. Sing et al. [17] evaluated on the relative density, microhardness and surface roughness of the L-PBF parts based on the varying of the laser power, scanning speed, as well as energy density. The result showed that laser power and scanning speed posed a significant effect on the density. However high energy density was required to obtain near full dense parts as sufficient thermal energy was introduced to fully melt the metal powders. And energy density might not be a good index to determine the quality of the L-PBF part. Gu et al. [18] conducted experiments and analysis to determine the influence of energy density on porosities and microstructure of the L-PBF parts. It was found out that test coupons fabricated using the same energy density with different laser powers and scanning speeds show significantly different degrees of porosity level. Other studies highlighted by Prashanth et al. [19] suggested energy density could be used as a guideline. Experimental and simulation results conducted by Criales et al. were shown that the process parameters (such as laser power and scanning speed) in laser powder bed fusion (L-PBF) affected the geometry of the melt pool and the presence of melt pools of varying size were definitely the key factors in microstructure characterisation and the calculation of mechanical properties of additively manufactured parts [20–22]. Further studies also showed that L-PBF parameters (laser power and scanning speed) might act as a physical metallurgy method to modify the microstructure of the AM printed parts which affected the mechanical properties [23–25].

For decades, the researchers working in L-PBF are perplexed by the strong anisotropy of samples microstructures which represent large columnar grains in the building directions. Some studies [26] focus on promoting the equiaxed grains and limiting the columnar grains by adjusting the process parameters to control the temperature gradient (G) and solidification velocity (R). However, this method always accompanies with lower scanning speed and laser power resulting in a long building time. Recently, equiaxed solidifications is greatly promoted by implementing a dense heterogeneous nucleation sites via powder surface treatment [27]. In addition, proper selection of postprocess measures (heat treatment) also can effectively induce the equiaxed grains and control the anisotropy of the microstructures [28].

With these, the authors realised that there is no definite relationship between the process parameters and the quality of the L-PBF part. The authors believed that geometry accuracy should be one of the key focus areas to determine the quality of the L-PBF part. And the geometry accuracy is dependent on the thermal behaviour in the L-PBF process.

The solidification process has impact on the microstructure evolution in the L-PBF process due to different thermal histories which pose an impact to the final property of the L-PBF parts. In addition, different process parameters will impact the geometry of melt pool differently which indirectly cause an effect on the strength and geometrical characteristics of the AM printed part as elaborated in Yadroitsev et al.[29]. Arisoy et al. presented on the influence of scan strategy and process parameters on microstructure in the aspect of the grain sizes which was correlated to the mechanical properties of the AM printed parts [30]. The mechanical properties are often used as a guideline for material qualification for metal additive manufacturing. The mechanical properties of materials are strongly depending on their underlying microstructure heterogeneity which includes the phase transformation, morphology and crystallography. The relationship between mechanical properties and microstructure is well related to the process parameters as microstructure is greatly affected by cooling and solidification rates which can be further optimised with specific processing parameters. The degree of an achievable quality optimisation in the AM process depends not only on process parameter optimisation (e.g., design of experiment), but also on the influence of the part geometry (e.g., shape and thickness) which is illustrated by Kok et al. [31]. Material process parameters such as material absorptivity and thermal properties have influential effect on the thermal history in the L-PBF process. Therefore, many efforts have conducted to study the link

between process parameters, thermal behaviour, and final quality in L-PBF, and to establish and understand process–structure–properties relationship. Yan et al. [32] proposed a process–structure–property prediction framework for the selective electron beam melting (SEBM) process. In the proposed framework, the processing materials data can be used to predict the material response and fatigue life of microstructure will be generated based on the relevant material response.

In the current research, a framework is introduced to link the AM process variables and part quality by identifying the process–structure–property–performance relationship in the AM process. In the framework as shown in Fig. 1, the AM process refers to powders characteristics and process parameters that affect the microstructure and property of the materials. Structure refers to the microstructure, grain growth and heterogeneity, and it depends mainly on how it is processed. Property refers to the strength and mechanical characteristic of the part fabricated by the AM process, which is illustrated the behaviour or reaction of the materials against external stimuli. Lastly, performance refers to the quality of the AM processed part and is mainly based on application uses. And material’s performance is a function on its properties. Thus, it is important to establish this relationship and the interrelationship amongst processing structure, properties and performance. Many numerical simulation are established to understand the AM process which includes temperature field, residual stress and mechanical properties. However, most models are not well connected and there is a gap in the understanding of the process–structure–property relationship. Therefore, this research focuses on understanding the process–microstructure–geometrical characteristic of the L-PBF process by experiment validation.

This paper aims to study microstructure evolution and microhardness based on the variation in the geometrical

Process-Structure-Property-Performance

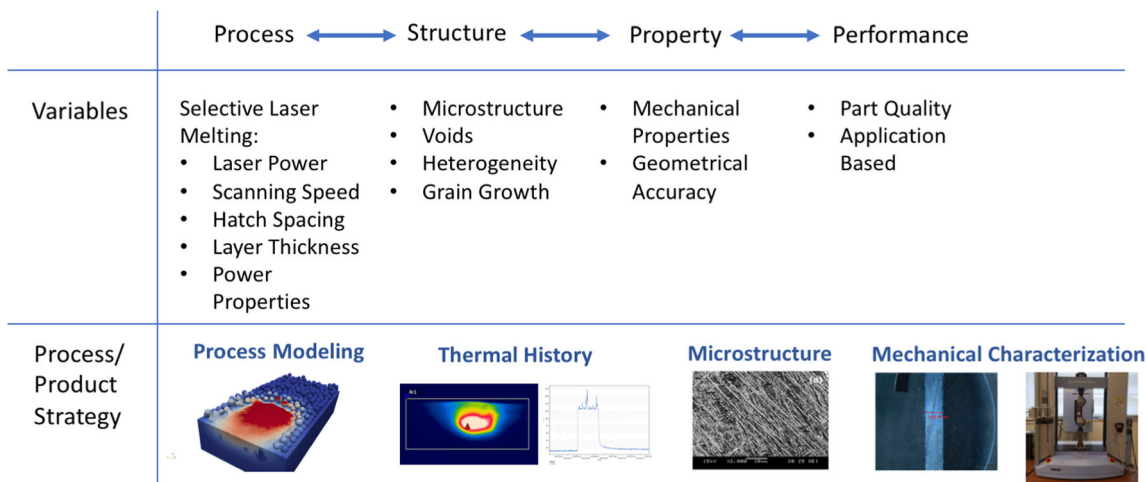


Fig. 1 A framework for integrated process–structure–property–performance for the AM process to directly connect process variables and process strategy

Table 1 The powder compositions of the Ti6AL4V and AlSi10Mg (Wt.%)

Ti6AL4V	Al	V	Fe	O	N	C	H	Ti	
	6.46	4.24	0.17	0.094	0.01	0.007	0.002	Bal.	
AlSi10Mg	Si	Mg	Fe	Mn	Cu	Zn	Sn	Ni	Al
	9–10	0.4–0.5	0.84	0.35	0.03	0.25	0.15	0.17	Bal.

characteristic of a L-PBF part and understand the link of the process parameters, thermal conductivity and mechanical properties in L-PBF. In this paper, two materials are selected: Ti6AL4V and AlSi10Mg alloys. Due to the difference in the thermal properties of the two materials, understanding of relationship between the geometrical effect and variation in thermal behaviour is required. The characterisation of mechanical properties and the geometric accuracy of the AM parts are considered as a function of variation in wall thickness, and are conducted by measuring the hardness and dimension of a L-PBF part. Investigation to observe the microstructure of L-PBF Ti6AL4V through scanning electron microscopy are also conducted.

It is important to establish the correlation between the geometrical characteristics, thermal properties of the materials, microstructure evolution and mechanical properties of the L-PBF part. The obtained findings can be used as design guidelines in micropart manufacturing such as the design of microlattice structures and provide a better unstinting of the L-PBF process capability.

The remainder of the paper is organised as follows. Section 2 provides details of experimental procedures with the L-PBF process and materials. Section 3 discusses the results and analysis of the proposed experiments in terms of wall thickness. Conclusions, limitations, and future work are presented in Section 4.

2 Experimental procedures

2.1 The L-PBF process

For this research, test samples were printed via the L-PBF process with a maximum power of 400W. The L-PBF machine used in this work is SLM 250HL (SLM Solutions Group AG, Lübeck, Germany). A dual laser system was employed, where the laser had a Gaussian profile for power inputs below 400 W and a top-hat profile for inputs up to 1 kW. The focused spot size was ~80 μm when the employed laser power was below 400W. During the fabrication process, recoater deposited powders across the build platform as it moved forward and backward. A laser beam scanned upon each layer of powders according to the stereolithography (STL) file. The build platform would move down with the lifting device by the designed thickness after each scan. A new layer of powder was then deposited by the recoater. This process repeated until the 3D object was fabricated. The materials were supplied by TLS Technik GmbH & Co. The compositions of Ti6AL4V and AlSi10Mg powders are shown in Table 1. The powders have nearly spherical morphology and the powder size ranges from 20 to 63 μm as shown in Fig. 2. In this experiment, the process parameters used in the L-PBF process was kept constant for geometry and mechanical properties characterisation as shown in Table 2. Stripes scanning strategy as shown in Fig. 3 was used.

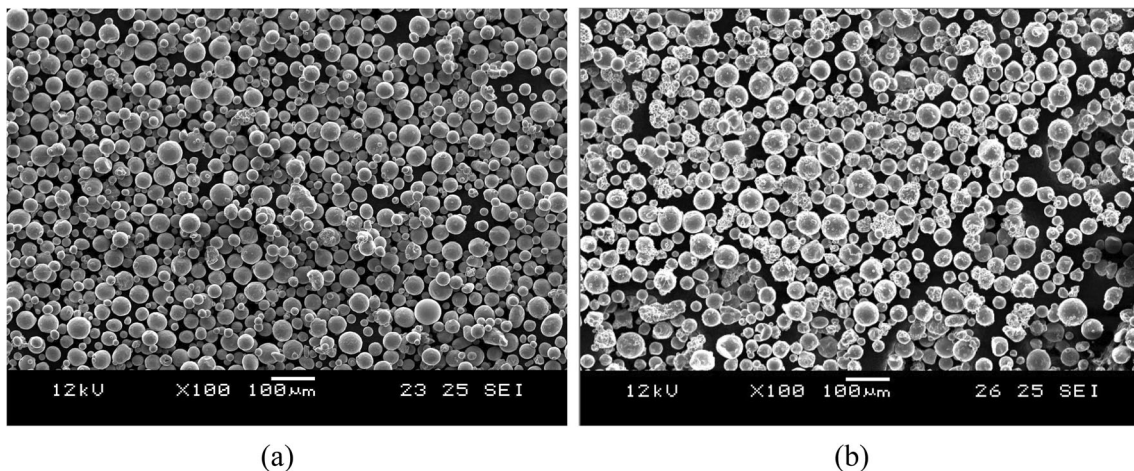
**Fig. 2** SEM images show the powder morphology of **a** Ti6AL4V and **b** AlSi10Mg

Table 2 Optimised process parameters for Ti6Al4V and AlSi10Mg alloy samples

Materials	Power (W)	Scanning speed (mm/s)	Hatch spacing (mm)	Layer thickness (mm)	Energy density (J/mm^3)
Ti6Al4V	95	125	0.11	0.050	138
AlSi10Mg	180	600	0.13	0.050	46

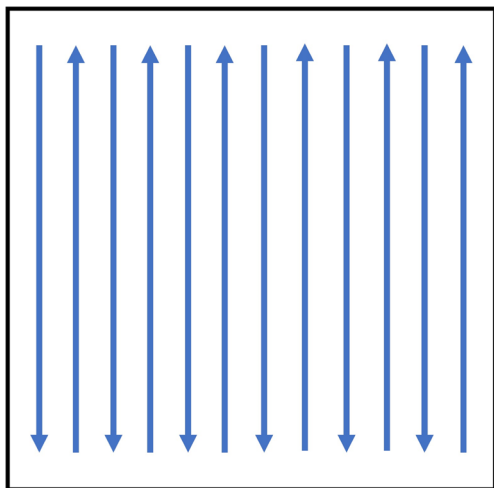
2.2 Specimen preparation

To investigate geometry accuracy and mechanical properties based on the variation in wall thickness types of block samples, varying wall thickness (0.3 to 3mm) were fabricated as shown in Fig. 4. The specimens were removed from the plate by CNC wire cutting machine and cold mounted with slow curing epoxy (EpoFix). Both Ti6Al4V and AlSi10Mg samples were polished using Struers Tegramin-25 polishing machine in accordance to the Struers protocol [33, 34]. The samples were etched using Kroll's and Keller's reagent to observe the microstructure and grain growth of Ti6Al4V and AlSi10Mg L-PBF samples respectively [35].

2.3 Geometrical accuracy and microhardness characterisation

Geometrical measurements in term of wall thickness and diameters were conducted at least five times using an OLYMPUS SZX7 optical microscope. Macrostructures and microstructures were investigated on the surface of the samples using a ZEISS Axioskop 2 MAT optical microscope and a Jeol JSM 5600-LV scanning electron microscope.

To determine the mechanical properties, vickers microhardness tests were conducted on the L-PBF-printed samples using a microhardness tester. The microhardness tests were conducted using a load of 300 g with 15 s hold time. The Vickers

**Fig. 3** Stripes strategy used in L-PBF

hardness test is mostly used for small parts and thin sections to measure the hardness of the materials which is suitable for the proposed research. Five test values were measured at different location along the direction of the wall as shown in Fig. 5. The mean value of the microhardness for each sample was obtained by averaging the measured test values.

3 Result and discussion

3.1 Geometrical accuracy due to variation in wall thickness

To understand the effect of the build geometry between the two materials with different thermal properties, the microstructure was studied along the X–Z plane. The results of the geometrical accuracy analysis with the variation in wall thickness of Ti–6Al–4V and AlSi10Mg were presented in Fig. 6, respectively.

Experimental result shows that wall thickness of 0.08 mm is unachievable and the minimum thickness to be achieved in the L-PBF process using Ti–6Al–4V is 0.2 mm. It is because a single scan path is generated within 0.08 mm wall thickness and the minimum wall thickness produced by a single laser scan is 0.2 mm. In a plot on the left side of Fig. 6(a), the fabricated wall thickness in Ti–6Al–4V are averagely larger than the designed wall thickness. This is mainly due to the high thermal energy input as mentioned in Yadroitsev et al. [10] and Thijs et al. [36], and high thermal energy is often associated with high power and low scanning speed. Figures 7 and 8 show the single L-PBF track width with various laser powers and scanning speeds. It is shown that variations in laser power and scanning speed produced different behaviour of the single track as shown in Fig. 9. The width of the single-track increases with the increasing of the laser power and decreasing of the scanning speed. With a high laser energy density, a huge volume of powder is involved in the track transformation; capillary and thermocapillary flows (the Marangoni effect) can significantly affect the geometry (increased width) of the track and its continuity. Furthermore, distortion was observed at low scanning speed as it requires a lot of energy to maintain the thermal change in the melted powder, the pressure produced by the vapour recoil causes distortion of the melted tracks as shown in Fig. 9. Whereas in the case of low laser energy density, there is a lack of laser energy and time to melt the metal powders which cause the

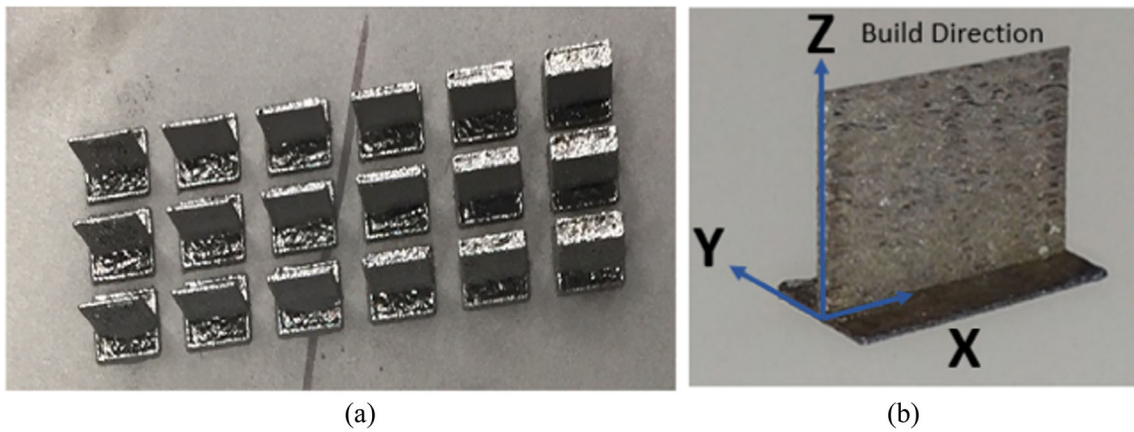
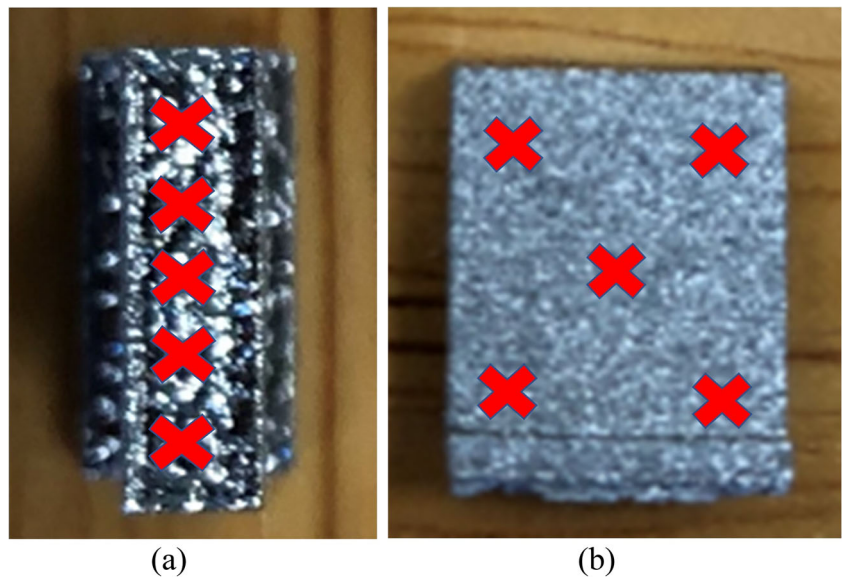


Fig. 4 **a** The Ti-6Al-4V samples as manufactured by L-PBF and **b** build orientation of the wall thickness fabricated by L-PBF

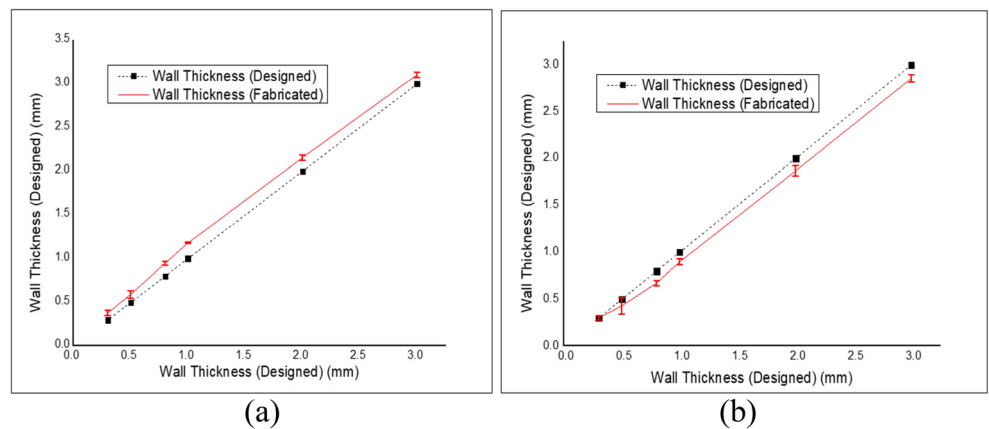
Fig. 5 Location of measurement for the study of geometric accuracy **(a)** and microhardness **(b)** due to variation in wall thickness



molten pool to become narrower. This instability behaviour will cause gaps or broken-line feature in-between the melted track as shown in Figs. 7 and 8.

As for AlSi10Mg, the fabricated wall thickness in AlSi10Mg are averagely smaller than the designed wall thickness. However, it is observed that there is a higher deviation

Fig. 6 Geometrical accuracy comparison of designed and fabricated **a** Ti-6Al-4V wall thickness and **b** AlSi10Mg wall thickness



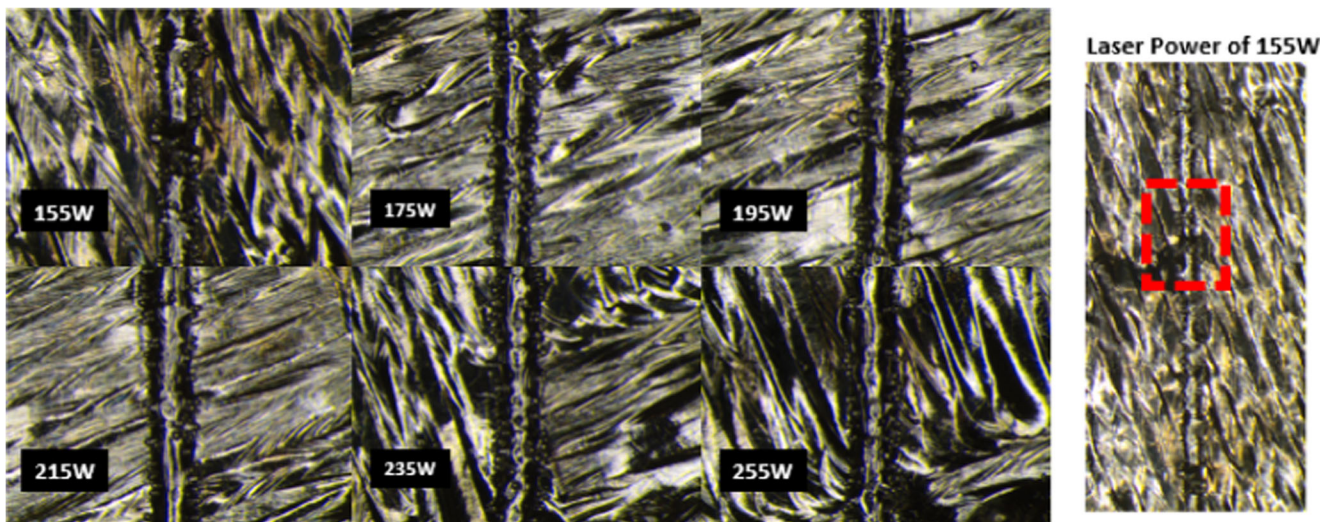


Fig. 7 Top view of the track width created with various laser powers from 155 to 215W

and inconsistency between fabricated and designed wall thickness in AlSi10Mg compared to Ti-6Al-4V as shown in Fig. 6(b). This is mainly due to the high thermal conductivity of the AlSi10Mg powder as excessive heat is transferred away from the melt pool and the formation of oxide layers on the top side of the melt track causing shrinkage during the L-PBF process. Studies on the feasibility of fabricating AlSi10Mg parts by L-PBF have also shown that it is difficult to control as compared to stainless steels and titanium alloys as supported by Aboulkhair et al. [37]. It is believed that a high laser power is preferred during the processing of AlSi10Mg with L-PBF, as this will compensate the high thermal gradient change due to the high thermal conductivity properties and scanning speed controls the width of the scan track resulting in geometrical accuracy. Comparison of the geometrical consistency in 1mm thickness between Ti-6Al-4V and AlSi10Mg was shown in Fig. 10. There are more uneven edges and lumps along the fabricated wall in AlSi10Mg as compared to Ti-6Al-4V.

3.2 Microstructure and microhardness due to variation in wall thickness

Figure 11 (a) shows the Vickers microhardness results from the 6 samples with varying wall thickness of Ti-6Al-4V and AlSi10Mg. In Ti-6Al-4V, the highest microhardness was found in the thinnest wall thickness (0.3mm) and microhardness decreased nonlinearly with the wall thickness. This phenomenon can be explained due to the change of cooling rate. In a thin wall, melt pool is surrounded by powders (like a thermally isolated condition) and effective energy density (removing transferred energy from input energy density) is higher than one in thicker wall. Peak temperature in the centre of melt pool results to high cooling rate. In more than 1.0 mm thickness, hardness was found to be stable in the range of 380–390 HV.

To understand the influence of build geometry on microhardness, the microstructure was analysed along the side plane as shown in Fig. 12. Figure 13 shows α/β phases microstructure from wall thickness of 0.3 to 3mm. The microstructure of

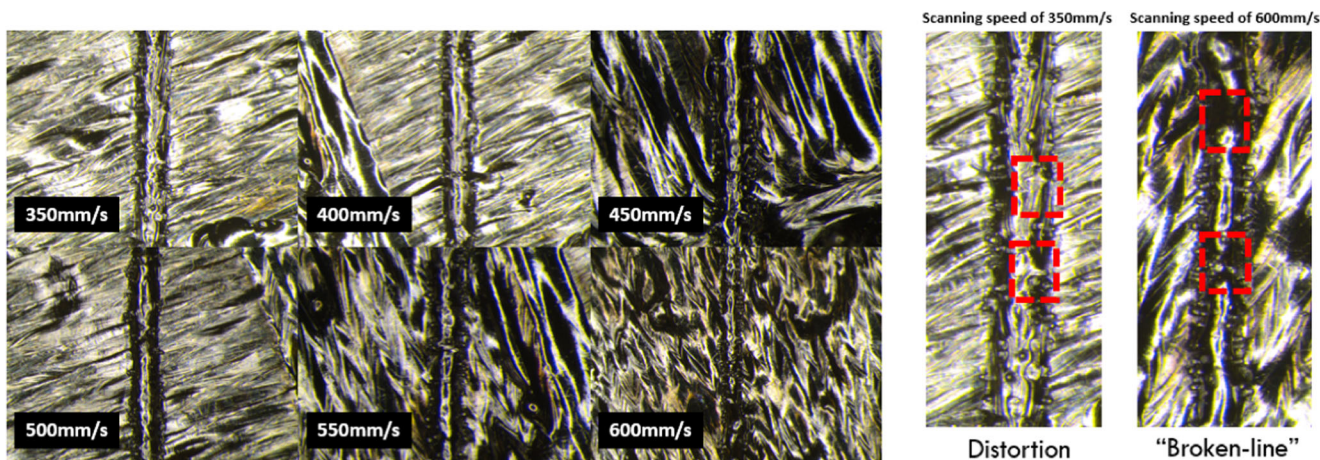


Fig. 8 Top view of the track width created with various scanning speeds from 350 to 600mm/s

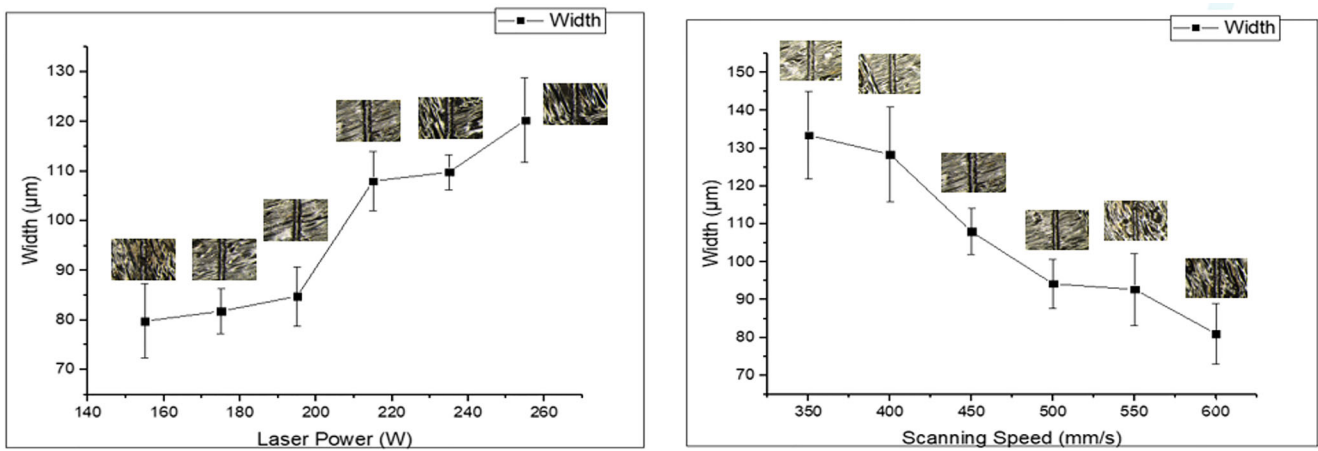


Fig. 9 Track width with respect to a laser power and b scanning speed

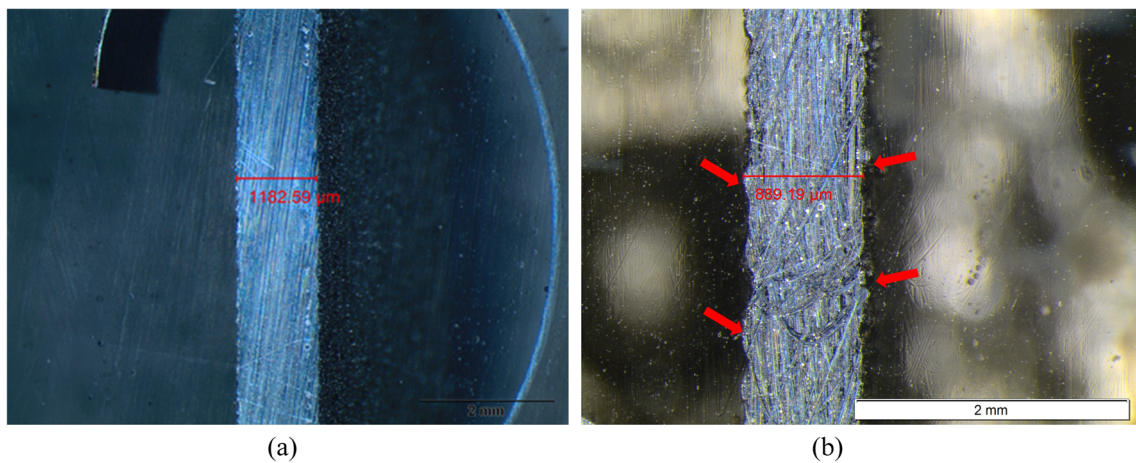


Fig. 10 Geometrical consistency in 1mm thickness between a Ti-6Al-4V and b AlSi10Mg

as-made samples by different wall thickness were generally similar: the samples had very fine acicular morphology which can be known as α' martensites. The martensitic

microstructure is a result of rapid solidification and cooling rate in the L-PBF process which are supported by Wauthle et al. [38] and Zhao et al. [39].

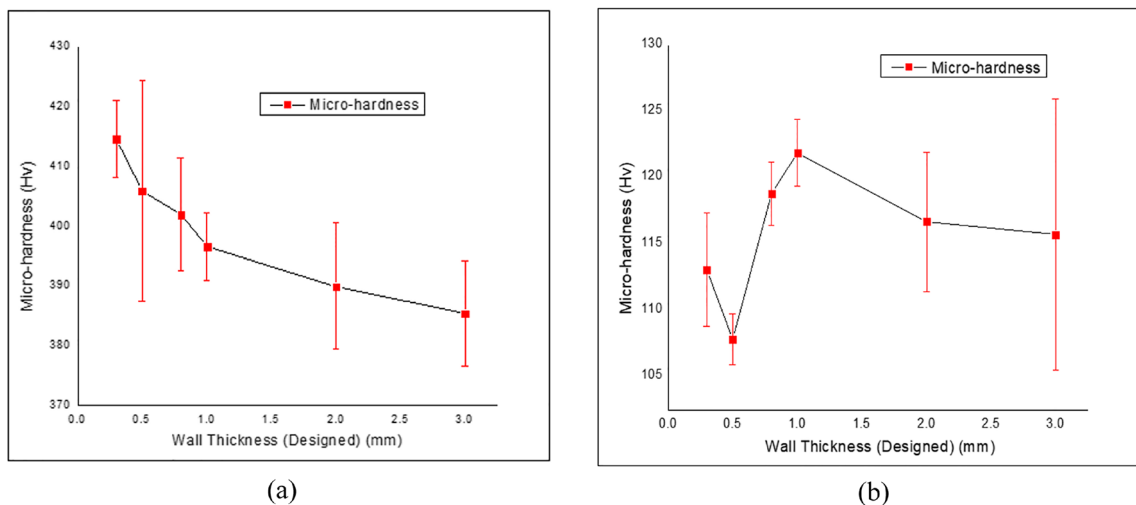


Fig. 11 Vickers microhardness of varying a Ti-6Al-4V wall thickness and b AlSi10Mg wall thickness

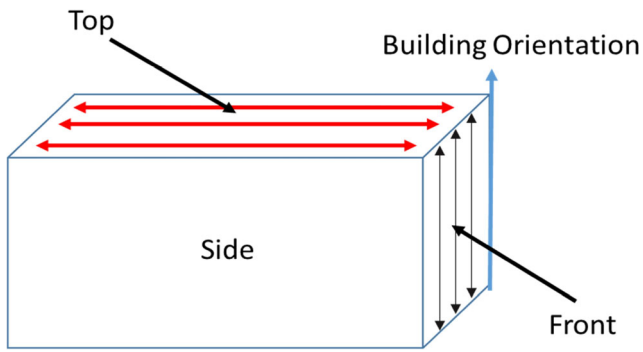


Fig. 12 Building orientation of the L-PBF part

However, the size and amount of α' martensites presence play an important part in influencing the microhardness. To clearly quantify the amount of α' martensites presented in the microstructure, original SEM images are converted into binary images and the comparison of microstructure between 0.3mm and 3mm wall thickness was presented in Fig. 14. It is observed that there are more α' martensites present in 0.3mm as compared to 3mm and this is mainly due to the discrepancies in thermal gradient and cooling rate. There is more scanning path found in 3mm and hence there are higher temperature within 3mm compared to 0.3mm. This will cause a decrease in the thermal gradient which result to in the decrease in α' martensites and microhardness. The relationship

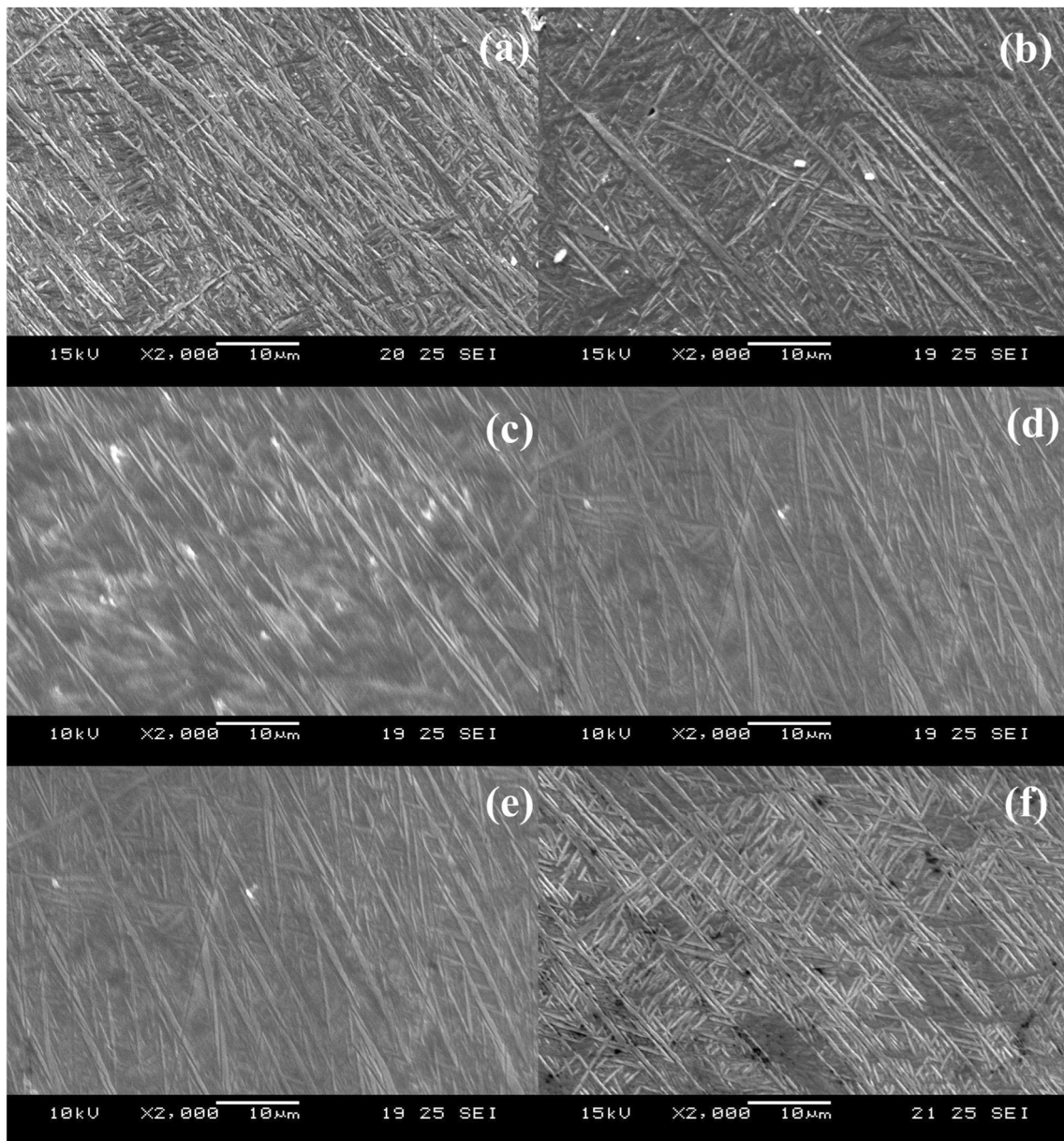
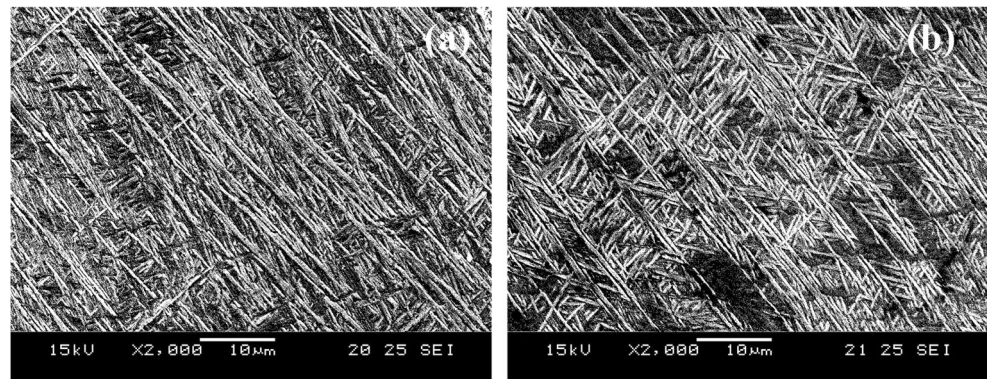


Fig. 13 SEM images showing the martensitic microstructure of Ti-6Al-4V wall thickness a 0.3mm, b 0.5mm, c 0.8mm, d 1mm, e 2mm, and f 3mm

Fig. 14 SEM binary images showing the microstructure of Ti–6Al–4V wall thickness **a** 0.3mm and **b** 3mm



between microhardness and α' martensites characteristics are well correlated with previous studies [40–46].

However, in the case of AlSi10Mg, there is no clear effect between the wall thickness and microhardness as shown in Fig. 9 (b). The microhardness of L-PBF AlSi10Mg was found to be (115.5 ± 7.5) Hv. Fast solidification during L-PBF produced fine microstructure with continuous Si segregation at the grain boundaries of the α -Al grains as shown in Fig. 15. The microstructure is much finer in wall thickness of 1mm as compared to the rest of the wall thickness and this is well correlated to the microhardness measured in wall thickness of 1mm.

In the case of Ti–6Al–4V, the result shows that the variation of thickness leads to the change of microhardness. The variation of hardness implies that the mechanical properties can be changed by the thickness. However, this phenomenon is not observed in AlSi10Mg and this can be understood that AlSi10Mg has a much higher thermal conductivity than Ti–6Al–4V. A higher thermal conductivity material will transfer, and release heat faster and hence provide lower thermal gradient as there is not much heat stored in the material during the L-PBF process. However, a low thermal conductivity material will conduct and transfer heat slower which result to a higher thermal gradient as there is a lot of heat stored in the material during the process.

4 Conclusion and future works

In this paper, L-PBF printed two different materials, Ti–6Al–4V and AlSi10Mg, with varying geometric factors were tested and studied for geometric accuracy and mechanical properties. We found that, in term of the geometric accuracy, AlSi10Mg was more difficult to control as compared to Ti–6Al–4V due to high thermal conductivity properties. Laser power and scanning speed were the key parameters to control the geometric accuracy. The microhardness of the fabricated samples was found that a directional decreasing trend with increasing wall thickness and the microhardness value would become constant in the range of 380–415HV. We attributed this trend to the behaviour change of the microstructure and the influence of a cooling rate. In term of the microhardness properties, the variation of thickness in Ti–6Al–4V had a greater effect on the microhardness due to the lower thermal conductivity properties and higher heat storage in the material during the L-PBF process.

In the introduced framework for the relationship of the integrated process–structure–property–performance (PSPP), the objective is to link the AM process variables and part quality. Simulation and modelling like complex process are extremely difficult to understand the relationship, due to the highly localised and material evolution that often occurs during the process. The results from the proposed experiment

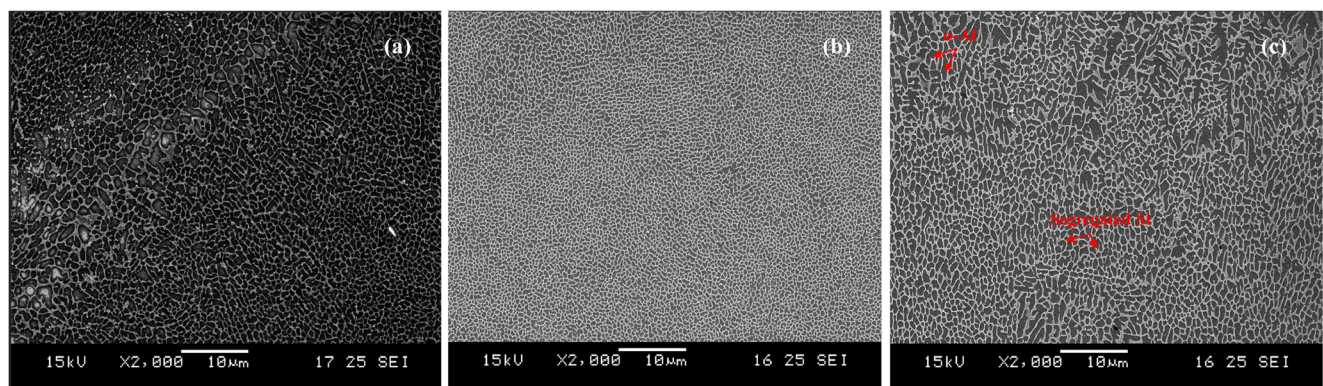


Fig. 15 SEM images showing the microstructure of AlSi10Mg wall thickness **a** 0.5mm, **b** 1mm, and **c** 3mm

show the effect and relationship between process parameters, material property, microstructure and microhardness property. And the results can be further applied to estimate the performance of materials in AM applications. However, the results are limited to microhardness properties, and there is a need to incorporate other mechanical tests such as tensile test into the proposed research. These studies can also be used as design guideline for lattice structure, as well as small-sized features, and the capability to control microstructure due to variation of geometrical factors.

Author contribution Conceptualisation—Zhong Yang Chua and II Hyuk Ahn

Formal analysis—Zhong Yang Chua, Lishi Jiao and Seung Ki Moon

Investigation—Zhong Yang Chua and II Hyuk Ahn

Methodology—Zhong Yang Chua, Lishi Jiao, II Hyuk Ahn and Seung Ki Moon

Supervision—Lishi Jiao, II Hyuk Ahn and Seung Ki Moon

Validation—Zhong Yang Chua and Lishi Jiao

Writing original draft—Zhong Yang Chua

Review and editing—Lishi Jiao, II Hyuk Ahn and Seung Ki Moon

Project administration—Seung Ki Moon

Funding acquisition—Seung Ki Moon and Lishi Jiao

Funding This research was supported by the Singapore Centre for 3D Printing (SC3DP), the National Research Foundation, Prime Minister's Office, Singapore, under its Medium-Sized Centre funding scheme, Natural Science Foundation of Hebei Province (Project No. F2020208018), and Funding for Introduction of Overseas Researcher of Hebei Province (Project No. C20190331).

Data availability The data and material are available upon request from the corresponding author.

Declarations

Ethics approval Not applicable.

Consent to participate Not applicable.

Consent for publication Not applicable.

Conflict of interest The authors declare that they have no conflict of interest.

References

- Moon SK, Tan YE, Hwang J, Yoon YJ (2014) Application of 3D printing technology for designing light-weight unmanned aerial vehicle wing structures. *International Journal of Precision Engineering and Manufacturing-Green Technology* 1(3):223–228
- Frazier WE (2014) Metal additive manufacturing: a review. *J Mater Eng Perform* 23(6):1917–1928
- Ko H, Moon SK, Hwang J (2015) Design for additive manufacturing in customized products. *Int J Precis Eng Manuf* 16(11):2369–2375
- Yao X, Moon SK, Bi G (2016) A cost-driven design methodology for additive manufactured variable platforms in product families. *J Mech Des* 138(4):041701
- Ahn IH, Moon SK, Hwang J, Bi G (2017) Characteristic length of the solidified melt pool in selective laser melting process. *Rapid Prototyp J* 23(2):370–381
- Dadbakhsh S., & Hao, L. (2014). Effect of layer thickness in selective laser melting on microstructure of Al/5 wt.% Fe₂O₃ powder consolidated parts. *The Scientific World Journal*, 2014.
- Koutiri I, Pessard E, Peyre P, Amlou O, De Terris T (2018) Influence of SLM process parameters on the surface finish, porosity rate and fatigue behavior of as-built Inconel 625 parts. *J Mater Process Technol* 255:536–546
- Liverani E, Toschi S, Ceschini L, Fortunato A (2017) Effect of selective laser melting (SLM) process parameters on microstructure and mechanical properties of 316L austenitic stainless steel. *J Mater Process Technol* 249:255–263
- Shi X, Ma S, Liu C, Chen C, Wu Q, Chen X, Lu J (2016) Performance of high layer thickness in selective laser melting of Ti6Al4V. *Materials* 9(12):975
- Yadroitsev I, Gusarov A, Yadroitsava I, Smurov I (2010) Single track formation in selective laser melting of metal powders. *J Mater Process Technol* 210(12):1624–1631
- Özel T, Altay A, Donmez A, Leach R (2018) Surface topography investigations on nickel alloy 625 fabricated via laser powder bed fusion. *Int J Adv Manuf Technol* 94(9-12):4451–4458
- Yadroitsev I, Smurov I (2011) Surface morphology in selective laser melting of metal powders. *Phys Procedia* 12:264–270
- Alghamdi A, Downing D, McMillan M, Brandt M, Qian M, Leary M (2019) Experimental and numerical assessment of surface roughness for Ti6Al4V lattice elements in selective laser melting. *Int J Adv Manuf Technol* 105(1-4):1275–1293
- Ch SR, Raja A, Jayaganthan R, Vasa NJ, & Raghunandan M (2020) Study on the fatigue behaviour of selective laser melted AISi10Mg alloy. *Mater Sci Eng A*, 139180.
- Yadroitsev I, Yadroitsava I, Bertrand P, Smurov I (2012) Factor analysis of selective laser melting process parameters and geometrical characteristics of synthesized single tracks. *Rapid Prototyp J* 18(3):201–208
- Li Y, Gu D (2014) Parametric analysis of thermal behavior during selective laser melting additive manufacturing of aluminum alloy powder. *Mater Des* 63:856–867
- Sing SL, Wiria FE, Yeong WY (2018) Selective laser melting of titanium alloy with 50 wt% tantalum: effect of laser process parameters on part quality. *Int J Refract Met Hard Mater* 77:120–127
- Gu H, Gong H, Pal D, Rafi K, Starr T, & Stucker B (2013) Influences of energy density on porosity and microstructure of selective laser melted 17-4PH stainless steel. In 2013 Solid Freeform Fabrication Symposium (Vol. 474).
- Prashanth KG, Scudino S, Maity T, Das J, Eckert J (2017) Is the energy density a reliable parameter for materials synthesis by selective laser melting? *Mater Res Lett* 5(6):386–390
- Criales LE, Arisoy YM, Özel T (2016) Sensitivity analysis of material and process parameters in finite element modeling of selective laser melting of Inconel 625. *Int J Adv Manuf Technol* 86(9):2653–2666. <https://doi.org/10.1007/s00170-0158329-y>
- Criales LE, Arisoy YM, Lane B, Moylan S, Donmez A, Özel T (2017) Predictive modeling and optimization of multi-track processing for laser powder bed fusion of nickel alloy 625. *Addit Manuf* 13:14–36. <https://doi.org/10.1016/j.addma.2016.11.004>
- Criales LE, Arisoy YM, Lane B, Moylan S, Donmez A, Özel T (2017) Laser Powder Bed Fusion of Nickel Alloy 625: Experimental investigations of effects of process parameters on melt pool size and shape with spatter analysis. *Int J Mach Tools Manuf* 121:22–36. <https://doi.org/10.1016/j.ijmactools.2017.03.004>

23. Cai C, Wu X, Liu W, Zhu W, Chen H, Qiu JCD, Sun CN, Liu J, Wei Q, Shi Y (2020) Selective laser melting of near- α titanium alloy Ti-6Al-2Zr-1Mo-1V: parameter optimization, heat treatment and mechanical performance. *J Mater Sci Technol* 57:51–64
24. Liu J, Song Y, Chen C, Wang X, Li H, Wang J et al (2020) Effect of scanning speed on the microstructure and mechanical behavior of 316L stainless steel fabricated by selective laser melting. *Mater Des* 186:108355
25. Larimian T, Kannan M, Grzesiak D, AlMangour B, Borkar T (2020) Effect of energy density and scanning strategy on densification, microstructure and mechanical properties of 316L stainless steel processed via selective laser melting. *Mater Sci Eng A* 770: 138455
26. Yan F, Xiong W, Faierson E (2017) Grain structure control of additively manufactured metallic materials. *Materials* 10:1260
27. Martin JH, Yahata BD, Hundley JM, Mayer JA, Schaedler TA, Pollock TM (2017) 3D printing of high-strength aluminium alloys. *Nature* 549:365–369
28. Vrancken B, Thijs L, Kruth J-P, Van Humbeeck J (2012) Heat treatment of Ti6Al4V produced by selective laser melting: microstructure and mechanical properties. *J Alloys Compd* 541:177–185
29. Yadroitsev I, Krakhmalev P, Yadroitsava I (2015) Hierarchical design principles of selective laser melting for high quality metallic objects. *Addit Manuf* 7:45–56
30. Ansoy YM, Criaes LE, Özel T, Lane B, Moylan S, Donmez A (2016) Influence of scan strategy and process parameters on microstructure and its optimization in additively manufactured nickel alloy 625 via laser powder bed fusion. *Int J Adv Manuf Technol*, 1-25.
31. Kok Y, Tan X, Tor SB, Chua CK (2015) Fabrication and microstructural characterisation of additive manufactured Ti6Al4V parts by electron beam melting: This paper reports that the microstructure and micro-hardness of an EMB part is thickness dependent. *Virtual Phys Prototyp* 10(1):13–21
32. Yan W, Lian Y, Yu C, Kafka OL, Liu Z, Liu WK, Wagner GJ (2018) An integrated process–structure–property modeling framework for additive manufacturing. *Comput Methods Appl Mech Eng* 339:184–204
33. Taylor B, & Weidmann E (2008) Metallographic preparation of titanium.
34. Weidmann E, & Guesnier A (2008) Metallographic preparation of aluminium and aluminium alloys.
35. Voort V, & George F (1999) Metallography, principles and practice, ASM Int. Mater. Park, Ohio, 487.
36. Thijs L, Verhaeghe F, Craeghs T, Van Humbeeck J, Kruth JP (2010) A study of the microstructural evolution during selective laser melting of Ti-6Al-4V. *Acta Mater* 58(9):3303–3312
37. Aboulkhair NT, Maskery I, Tuck C, Ashcroft I, Everitt NM (2016) On the formation of AlSi10Mg single tracks and layers in selective laser melting: microstructure and nano-mechanical properties. *J Mater Process Technol* 230:88–98
38. Wauthle R, Vrancken B, Beynaerts B, Jorissen K, Schrooten J, Kruth JP, Van Humbeeck J (2015) Effects of build orientation and heat treatment on the microstructure and mechanical properties of selective laser melted Ti6Al4V lattice structures. *Addit Manuf* 5: 77–84
39. Zhao X, Li S, Zhang M, Liu Y, Sercombe TB, Wang S, Hao Y, Yang R, Murr LE (2016) Comparison of the microstructures and mechanical properties of Ti-6Al-4V fabricated by selective laser melting and electron beam melting. *Mater Des* 95:21–31
40. Chen LY, Huang JC, Lin CH, Pan CT, Chen SY, Yang TL, Lin DY, Lin HK, Jang JSC (2017) Anisotropic response of Ti-6Al-4V alloy fabricated by 3D printing selective laser melting. *Mater Sci Eng A* 682:389–395
41. Kok YH, Tan XP, Loh NH, Tor SB, Chua CK (2016) Geometry dependence of microstructure and microhardness for selective electron beam-melted Ti-6Al-4V parts. *Virtual Phys Prototyp* 11(3): 183–191
42. Yang J, Yu H, Yin J, Gao M, Wang Z, Zeng X (2016) Formation and control of martensite in Ti-6Al-4V alloy produced by selective laser melting. *Mater Des* 108:308–318
43. Yang J, Han J, Yu H, Yin J, Gao M, Wang Z, Zeng X (2016) Role of molten pool mode on formability, microstructure and mechanical properties of selective laser melted Ti-6Al-4V alloy. *Mater Des* 110:558–570
44. Li C, Sun S, Zhang Y, Liu C, Deng P, Zeng M, Wang Y (2019) Effects of laser processing parameters on microstructure and mechanical properties of additively manufactured AlSi10Mg alloys reinforced by TiC. *Int J Adv Manuf Technol* 103(5-8):3235–3324
45. Han Q, Jiao Y (2019) Effect of heat treatment and laser surface remelting on AlSi10Mg alloy fabricated by selective laser melting. *Int J Adv Manuf Technol* 102(9-12):3315–3324
46. Dong Z, Liu Y, Li W, Liang J (2019) Orientation dependency for microstructure, geometric accuracy and mechanical properties of selective laser melting AlSi10Mg lattices. *J Alloys Compd* 791: 490–500

Publisher's note Springer Nature remains neutral with regard to jurisdictional claims in published maps and institutional affiliations.